

Article

Effect of Rice Straw on Tensile Properties of Tailings Cemented Paste Backfill

Zeyu Li, Xiuzhi Shi and Xin Chen * 

School of Resources and Safety Engineering, Central South University, Changsha 410083, China; lizeyu@csu.edu.cn (Z.L.); baopo@csu.edu.cn (X.S.)

* Correspondence: chenxin_ck@csu.edu.cn; Tel.: +86-15116336263

Abstract: It is important and difficult to improve the tensile strength of backfill material to ensure the stability of goafs. In this study, rice straw (RS) in fiber form is used to improve the tensile properties of cemented paste backfill (CPB). An orthogonal experiment was designed, Brazilian indirect tensile strength tests were conducted to test the tensile performance of RS fiber-reinforced cemented paste backfill (RSCPb) under different fiber content (1, 2, 3 kg/m³) and fiber length (0.8~1, 1~3, 3~5 cm), and the microstructure of RSCPb was analyzed with scanning electron microscopy (SEM). The results showed that, compared with the conventional cemented paste backfill (CCPB), the increase in tensile strength of RSCPb ranged from 115.38% to 300.00% at 3 days curing age, 40.91% to 346.15% at 7 days, and -38.10% to 28.00% at 28 days, and the strain was slightly reduced during the curing period. The tensile strength, strain, and percentage increase of the RSCPb compared to the CCPB did not show a monotonic pattern of variation with the RS fiber content and length during the curing period. The RSCPb samples fractured under peak stress, showing obvious brittle failure. In addition, sulfate generated from S²⁻ in the tailings inhibits the hydration reaction, and generates swelling products that form weak structural surfaces, which, in turn, lead to a 28-day tensile strength and strain of RSCPb lower than those at 7 days.

Keywords: rice straw fiber; cemented paste backfill; Brazilian test; orthogonal experiment; tensile strength; tensile strain



Citation: Li, Z.; Shi, X.; Chen, X. Effect of Rice Straw on Tensile Properties of Tailings Cemented Paste Backfill. *Appl. Sci.* **2022**, *12*, 526. <https://doi.org/10.3390/app12010526>

Academic Editors: Yeonho Park and Young Hoon Kim

Received: 13 November 2021

Accepted: 30 December 2021

Published: 5 January 2022

Publisher's Note: MDPI stays neutral with regard to jurisdictional claims in published maps and institutional affiliations.



Copyright: © 2022 by the authors. Licensee MDPI, Basel, Switzerland. This article is an open access article distributed under the terms and conditions of the Creative Commons Attribution (CC BY) license (<https://creativecommons.org/licenses/by/4.0/>).

1. Introduction

In the underground mining process, filling the goafs with cemented paste backfill (CPB) mixed with tailings, cement, and water is an effective way to control ground pressure and treat mining waste [1–3]. However, limited by the properties of tailings and the cost of cement, the strength of CPB is usually quite low, especially the tensile strength. It is only about one-tenth of the compressive strength, and low tensile strength becomes an important hidden danger that causes damage to CPB [4]. Generally, the properties of specific tailings produced by mines are difficult to change. Increasing the usage of cement has become the main method to enhance the strength of CPB, which greatly increases the backfill cost of the mining enterprise [5]. How to improve the tensile strength of CPB economically and effectively is a topic of concern to related researchers. Driven by the demand, some scholars have studied the impact of using fibers, rubber crumbs, and nanomaterials as additives on backfill materials or cementitious materials [6–8]. Zhu et al. [9] incorporated glass fibers into shotcrete, and the results showed that the maximum tensile strength of the shotcrete added with glass fibers reached more than 300%, and the maximum increase in shear strength reached more than 500%. Chen et al. [10,11] studied the compressive properties, tensile properties, and microstructure of polypropylene fiber-reinforced CPB, and found that polypropylene fibers can enhance the stiffness and ductility of CPB, improve the residual strength of CPB after destruction, and reduce the porosity of CPB. Cristelo et al. [12] found that the strength and strain of cement-stabilized sandy-clay

increased with the increase in polypropylene fiber content under indirect tensile stress. Juradin et al. [13] found that Spanish broom fibers can significantly improve the ductility of cementitious materials. Jiang et al. [14] found that concrete with basalt fibers significantly increased the tensile strength, flexural strength and toughness index. Long et al. [15] added Masson pine needle fibers to the concrete and found that the modulus of rupture, toughness index, and deflection of concrete could be improved by a maximum of 46.1%, 40%, and 129% respectively. Mansouri et al. [16] improved the compressive strength and abrasive resistance of concrete by mixing steel fibers into concrete. These fiber materials have the advantages of high strength and good ductility, and adding fiber material is an effective method to improve the properties of cementitious materials [17,18]. In general, natural fibers are more readily available than man-made organic and metallic fibers, especially plant fibers. However, the application of rice straw (RS) fiber, as an environmentally friendly and easily available material, in the field of mine backfill has rarely been reported.

In agricultural production, a large amount of wheat straw and rice straw is abandoned or burned every year [19]. Although incineration in situ is economical and labor saving, it causes air pollution. In addition, they can also be used to generate electricity [20], make paper, fodder, or fertilizer [21,22]. In some areas, straw and soil were used as construction materials. The addition of rice husks to lightweight concrete provided excellent mechanical and thermal properties, making it suitable for use as a building material [23]. Rice stalk bales could be used to build high-performance, environmentally friendly building walls [24]. Studies show that RS cement specimens meet the strength requirements of ASTM standard [25], and RS could significantly reduce the cost of cement bricks and the greenhouse gas emissions from cement production while achieving the same strength [26]. The elasticity modulus and compressive strength of the cementitious materials' specimens made with RS were also enhanced [26,27]. These studies show that adding RS fibers into CPB is not only feasible but also environmentally friendly and cost effective. The tensile properties of CPB deserve to be explored as an aspect of its mechanical properties, but there are few studies related to the tensile properties of CPB with RS fibers added. Some scholars have studied the properties of the composites of RS fibers and cementitious materials and found that the rod-shaped RS can enhance the indirect tensile strength of the cemented tailings backfill [28]. However, they have only explored the effect of RS length and did not take into account the RS content, and the study was conducted on rod-shaped RS not the fibrous form. The paucity of tensile properties of RS fiber-reinforced cemented paste backfill (RSCPB) hinders its application, and the tensile performance of RSCPB still needs to be further investigated.

In summary, it is feasible to improve the tensile strength of filling by adding fiber materials, however, there are few reports on the use of RS fibers to achieve this goal. Compensating for the lack of research on the tensile performance of CPB by fibrous forms of RS fibers is necessary. Therefore, this research uses the Brazilian split method to test the tensile strength performance of CPB after adding RS, analyzes the instability mode of RSCPB through the macro and micro method, and studies the effect of RS parameters on the tensile strength of CPB.

2. Materials and Methods

2.1. Material Property

The lead–zinc tailings for the preparation of RSCTB specimens in this research were obtained by filtering the overflow water of the cyclone thickener, and the cement used in this experiment was ordinary Portland cement P.O 42.5R. Table 1 and Figure 1 show the density and particle size distribution of lead–zinc tailings and cement. LS particle size analysis results indicated that the median diameter D_{50} of tailings was 25.31 μm and the percentage of tailings particles smaller than 0.074 mm accounted for 85.8%. It is generally believed that fine particles hinder the dewatering of the backfill and reduce CPB strength [29,30]. According to Figure 1 and Table 1, the gradation curves of cement particles are smooth. However, the curvature coefficient of tailings is less than 1 and the

uniformity coefficients are greater than 10, which indicates that the gradation of tailings is not well-graded. X-ray fluorescence spectroscopy (XRF) is often used to determine chemical composition [31], and the results are shown in Table 2. The tailings contain 27.1% SiO₂ and 22.6% CaO (Table 2), which are the main chemicals required for cement hydration reaction.

Table 1. Main properties of tailings and cement.

Physical Property	Particle Density ρ_s (t/m ³)	D_{10} (μm)	D_{30} (μm)	D_{50} (μm)	D_{60} (μm)	Uniformity Coefficient C_u ¹	Curvature Coefficient C_c ²
Tailings	3.34	3.21	9.82	25.31	33.01	10.3	0.91
Cement	3.11	2	6.54	13.65	17.82	8.9	1.2

¹ $C_u = D_{60}/D_{10}$; ² $C_c = (D_{30})^2 / (D_{10} \times D_{60})$.

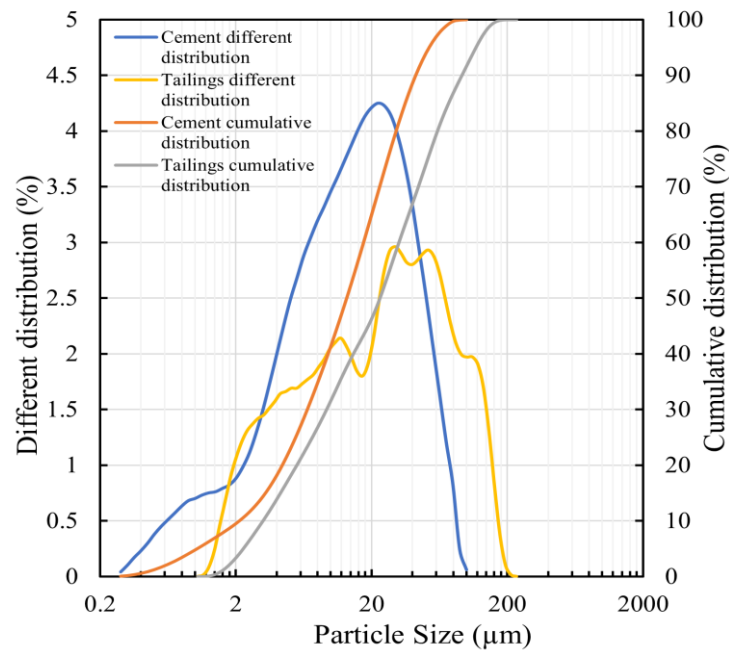


Figure 1. Particle size distribution of cement and tailings.

Table 2. Main composition of cement and tailings.

Main Chemical Composition	Tailings	Cement	Unit
SiO ₂	27.1	19.76	%
Al ₂ O ₃	9.11	4.93	%
Fe _x O _y	23.7	3.27	%
CaO	22.6	59.88	%
S ²⁻	11.9	3.78	%
K ₂ O	2.19	0.98	%
MgO	1.40	1.39	%
TiO ₂	0.26	0.25	%
Na ₂ O		0.27	%
Cl	0.01	0.022	%
P ₂ O ₅	0.08	0.07	%
MnO	0.01	0.073	%
Zn	0.43		%
Pb	0.88		%
Cr	0.01		%
Ni	0.012		%
Ba	0.07		%
Zr	0.007		%
As	0.098		%
Rb	0.006		%
Cu	0.032		%
Sr	0.014		%
Others	0.081	5.325	%

The main properties of RS fibers are listed in Table 3. The tensile strength of the RS fiber is 5.4 MPa, and its elongation is 2.3% [32]. In addition, RS fibers have a dry density of only 85 kg/m³ and a water absorption capacity of 300–517% [26]. Three lengths of RS fiber (Figure 2) were used in this experiment. Tap water was also used for the experiments.

Table 3. Main properties of RS fibers [27,33].

Chemical Constituent	Cellulose	Hemicellulose	Lignin	Ash	Moisture
Weight Percentage (%) Wet matter	35.6	20.5	16.8	15.2	11.9
Chemical Constituent	N	P ₂ O ₅	K ₂ O	S	Si
Weight Percentage (%) Dry Matter	0.5~0.8	0.16~0.27	1.4~2.0	0.05~0.10	4~7



Figure 2. The morphology of RS fibers.

2.2. Experimental Design and Specimen Preparation

Two groups of tests, A and B, were designed, in which different qualities and lengths of RS fibers were added to the specimens of group A, as shown in Table 4. Group B was a control group of conventional cemented paste backfill (CCPB) without RS fibers. According to the 4-factor and 3-level orthogonal test $L_9(3^4)$, nine formulas were designed for group A. The factors included cement content (c : 25, 20, and 17%), solid mass concentration (ω : 60, 62, and 64%), fiber addition (m : 1, 2, 3 kg/m³), and fiber length (l : 0.8~1, 1~3, 3~5 cm). The cement content of 25%, 20%, and 17% corresponded to cement–tailings ratios of 1:4, 1:5, and 1:6. After permutation and combination, nine types of water cement ratios 3.33 (c : 25%, ω : 60%), 3.06 (c : 25%, ω : 62%), 2.81 (c : 25%, ω : 64%), 4.00 (c : 20%, ω : 60%), 3.68 (c : 20%, ω : 62%), 3.38 (c : 20%, ω : 64%), 4.67 (c : 17%, ω : 60%), 4.29 (c : 17%, ω : 62%), 3.94 (c : 17%, ω : 64%) were calculated. The selection of cement content and solid mass concentration was based on the parameters currently used by tailings source mine enterprise. Orthogonal experiment method was chosen to simplify the complete experiment with multiple factors that require complex manipulations, in order to improve the efficiency of the experiment and to obtain the best formulation quickly. Group B was a full-scale experiment with two factors including cement content and solid mass concentration and three levels, the results of which have been discussed in the literature [4].

The temperature and humidity of the curing environment are important factors affecting the reliability of concrete structures, and suitable maintenance conditions help to obtain accurate and reliable strength data [34,35]. After the raw materials were fully stirred by a mortar mixer for 10 min, the fresh slurry was stored in a mold of size $\phi 50 \text{ mm} \times 50 \text{ mm}$ and cured in an environment of $22 \pm 1 \text{ }^\circ\text{C}$ and 90% relative humidity.

RS fibers showed slight side effects of a decrease of 5% in the flowability of the fresh CTB slurry because RS fibers with high water absorption cause viscous increases in the fresh CTB slurry. In spite of this, the flowability of the RSCPb met the pipeline transportation requirements.

Table 4. Orthogonal table $L_9(3^4)$ of all manufactured mixtures.

Specimen Number	Cement Content c (%)	Solid Mass Concentration ω (%)	Fiber Content m (kg/m ³)	Fiber Length l (cm)	Specimen Number	Cement Content c (%)	Solid Mass Concentration ω (%)
A1	25	60	1	0.8~1	B1	25	60
A2	25	62	2	1~3	B2	25	62
A3	25	64	3	4~5	B3	25	64
A4	20	60	2	1~3	B4	20	60
A5	20	62	3	4~5	B5	20	62
A6	20	64	1	0.8~1	B6	20	64
A7	17	60	3	0.8~1	B7	17	60
A8	17	62	1	1~3	B8	17	62
A9	17	64	2	4~5	B9	17	64

¹ Ratio of the weight of cement to the sum of the weight of cement and tailings; ² Ratio of the weight of all solids to the total weight of the mixture.

2.3. Brazilian Split Test

The Brazilian test is widely regarded as an effective indirect tensile strength (ITS) test method often used for the tensile testing of rocks and composites [36], in which two thin steel bar pads are placed parallel to the cylinder and perpendicular to the diameter direction of the cylindrical specimen, and linear loads are applied from the upper and lower sides to fracture it along the radial direction (Figure 3a) [37]. When the disc specimen is subjected to a concentrated radial load, it can be simplified to a plane strain problem in elastic mechanics. According to the elastic mechanics theory, the tensile stress at the center of the disc when it fails is the ITS of the specimen. The Brazilian split test can ensure that the tensile force passes through the center of the specimen being tested. In this experiment, the WHY-200 fully automatic pressure testing machine was used to test the specimens cured for 3 days, 7 days, and 28 days. The tensile strength of the specimen in the Brazilian split test can be calculated by Equation (1) [4]

$$\sigma_t = -2P / \pi dt \tag{1}$$

where P is the applied vertical load, d is the disc specimen diameter, and t is the disc specimen thickness.

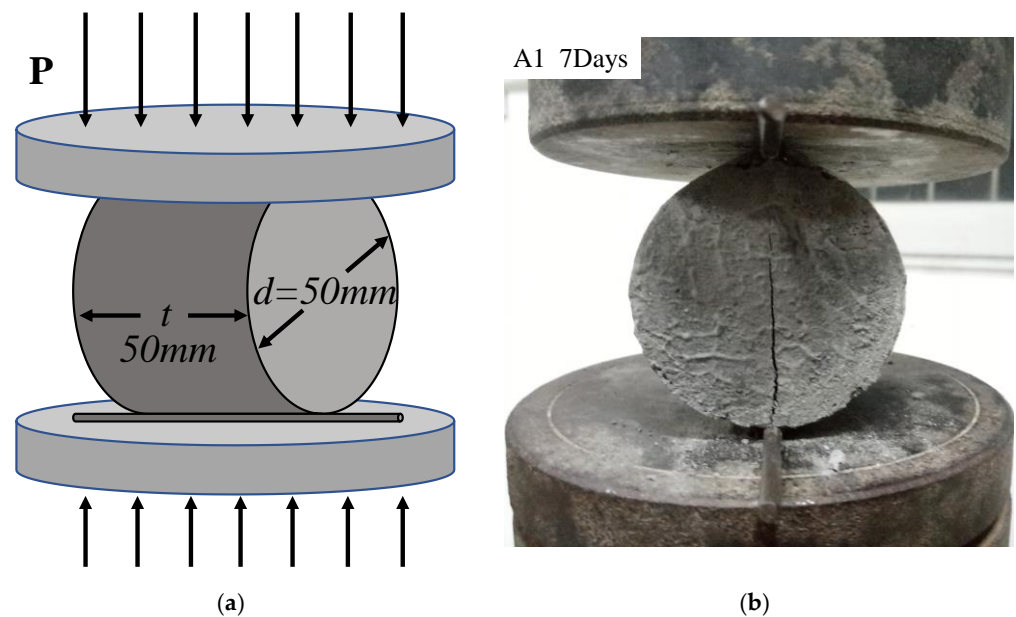


Figure 3. (a) The Brazilian split test. (b) Tensile failure of test specimen A1 curing for 28 days.

2.4. Scanning Electron Microscopy (SEM)

Microscopic analysis helps to investigate the mode and effect of the binding of RS fibers with hydration products of cement and tailings. SEM analysis was performed on the specimens after 28 days of curing, and the compositions of the hydration products were also analyzed using the accompanying X-ray energy dispersive spectrometry (EDS) equipment.

3. Results and Discussion

3.1. CPB Failure Process

Brazilian split tensile tests were carried out on the specimens prepared in accordance with Table 4. As shown in Figure 3b, all specimens were broken vertically along the diameter direction and fracture failure occurred.

Figure 4 shows the tensile stress–strain curves of RSCPb and CCPb. From the stress–strain curves, the following can be found:

- (1) The peak tensile stress (σ_t) of RSCPb is generally higher than that of CCPb. However, the peak tensile strain (ϵ) of most RSCPb specimens is lower. From the stress–strain relationship, both CCPb and RSCPb exhibit obvious brittle failure characteristics and basically satisfy the tensile loading failure process of brittle materials, as shown in Figure 5. The stress–strain relationship passes through four phases during the process from loading to failure: OA-linear elastic phase; AB-yielding phase; BC-failure phase, characterized by stress drop; CD post-failure phase. However, some of the specimens showed no residual strength and even fractured directly after the tensile force exceeded the ultimate stress, and the stress dropped to 0 MPa.
- (2) In the pre-peak phase, RSCPb specimens have a greater elastic modulus. Although relatively small critical deformation limits the deformation energy that the RSCPb can withstand and inhibits its toughness development, the RSCPb specimens possess enhanced toughness performance under the same strength or deformation, which is important for preventing mine stratigraphic displacement and maintaining ground pressure stability. Therefore, RSCPb has a promising application prospect.
- (3) In the post-peak phase, stress drops occurred in all CPb specimens when the stress exceeded the peak tensile strength, indicating that CPb fractured under a tensile stress load, and CPb failed instantaneously and completely. CCPb showed almost no residual strength. A part of RSCPb specimens showed a slow stress drop and retained residual strength, which indicates that the RS fibers play a positive role in connecting the damaged parts and improving their residual strength during the tensile damage of the specimens.

3.2. Influence of Cement Content and Solid Mass Concentration

Table 5 lists the Brazilian split ITS results and peak tensile strain statistics of RSCPb (Group A) and CCPb (Group B). Based on orthogonal analysis of ITS (σ_t) and peak tensile strain (ϵ), the range R of average values of σ_t and ϵ at each level was obtained. The larger R is, the greater the effect of the variation in the value of this factor on the results is. According to the analysis results shown in Table 6, cement content is the factor that has the greatest impact on strength and strain in different curing periods. This is because the cement content is directly related to the amount of hydration products. The results also show that the importance of solid mass concentration and RS fibers parameters change with increasing curing time, and that the RS parameter is no less important than the solid mass concentration.

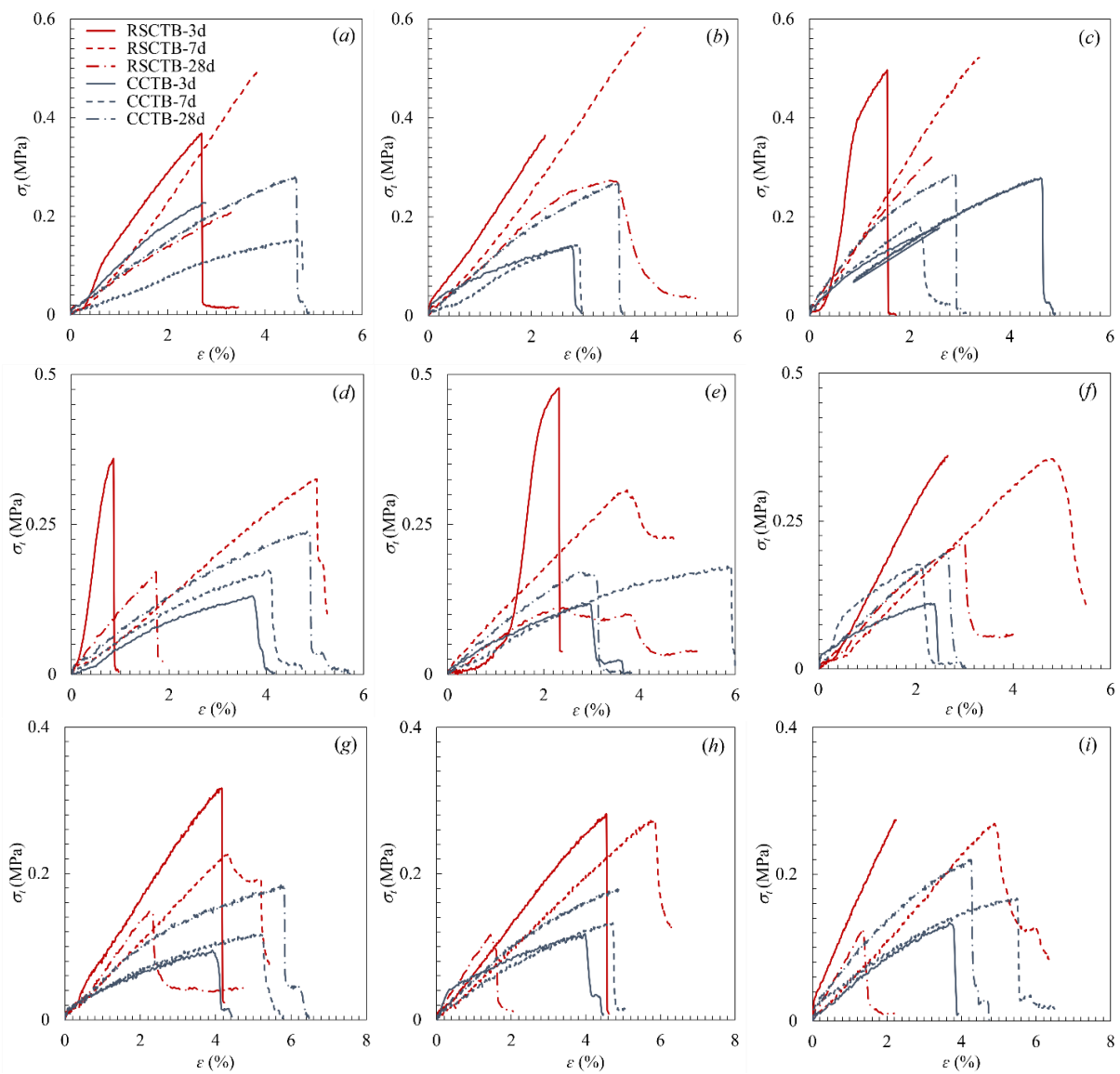


Figure 4. Stress–strain curves obtained from the Brazilian tests. (a–i) represent nine formulas in Table 4 respectively.

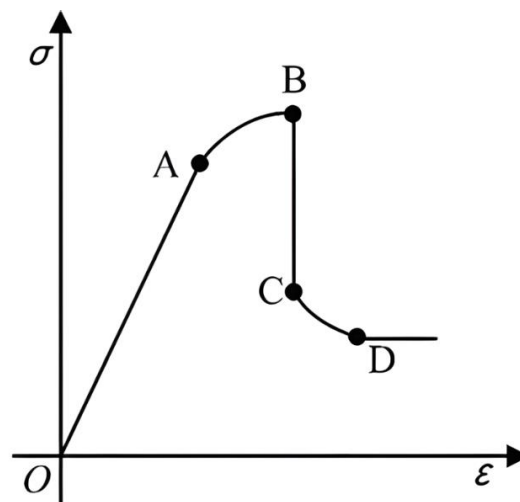


Figure 5. Tensile stress–strain curve of brittle materials.

Table 5. ITS and peak tensile strain results of RSCP (Group A) and CCPB (Group B).

Number	ITS σ_t (MPa)			Peak Strain ϵ (%)		
	3d	7d	28d	3d	7d	28d
A1	0.37	0.50	0.21	2.69	3.90	3.30
A2	0.36	0.58	0.27	2.26	4.19	3.67
A3	0.50	0.53	0.32	1.55	3.39	2.50
A4	0.36	0.33	0.17	0.86	5.03	1.73
A5	0.48	0.31	0.11	2.31	3.74	2.38
A6	0.36	0.36	0.21	2.65	4.75	3.01
A7	0.32	0.23	0.15	4.16	4.34	2.34
A8	0.28	0.27	0.12	4.56	5.87	1.44
A9	0.28	0.27	0.13	2.25	4.87	1.38
B1	0.23	0.14	0.25	2.78	4.76	4.64
B2	0.14	0.13	0.26	2.78	2.93	3.70
B3	0.18	0.18	0.25	4.64	2.16	2.92
B4	0.13	0.17	0.22	3.72	4.09	4.88
B5	0.12	0.22	0.16	3.00	5.91	3.09
B6	0.11	0.15	0.22	2.38	2.15	2.67
B7	0.10	0.12	0.16	3.88	5.23	5.82
B8	0.12	0.13	0.19	3.93	4.72	4.91
B9	0.13	0.18	0.21	3.73	5.50	4.27

Table 6. Orthogonal range analysis results.

Property	Curing Age	Level	<i>c</i>	ω	<i>m</i>	<i>l</i>	Significance
σ_t	3d	k_1	0.410	0.350	0.337	0.377	$c > m > l > \omega$
		k_2	0.400	0.373	0.333	0.347	
		k_3	0.293	0.380	0.433	0.380	
		<i>R</i>	0.117	0.030	0.100	0.033	
	7d	k_1	0.537	0.353	0.377	0.360	$c > m > \omega > l$
		k_2	0.333	0.387	0.393	0.390	
		k_3	0.257	0.387	0.357	0.377	
		<i>R</i>	0.280	0.034	0.036	0.030	
	28d	k_1	0.267	0.177	0.180	0.150	$c > l > \omega > m$
		k_2	0.163	0.167	0.190	0.210	
		k_3	0.133	0.220	0.193	0.203	
		<i>R</i>	0.134	0.053	0.013	0.060	
ϵ	3d	k_1	2.167	2.570	3.300	2.417	$c > m > \omega > l$
		k_2	1.940	3.043	1.790	3.023	
		k_3	3.657	2.150	2.673	2.323	
		<i>R</i>	1.717	0.893	1.510	0.700	
	7d	k_1	3.827	4.423	4.840	4.170	$c > m > l > \omega$
		k_2	4.507	4.600	4.697	4.427	
		k_3	5.027	4.337	3.823	4.763	
		<i>R</i>	1.200	0.263	1.017	0.593	
	28d	k_1	3.157	2.457	2.583	2.353	$c > l > m > \omega$
		k_2	2.373	2.497	2.260	3.007	
		k_3	1.720	2.297	2.407	1.890	
		<i>R</i>	1.437	0.200	0.323	1.117	

It can be seen from Figure 6a that the stress decreases monotonously with decreasing cement content, which is the same as the conclusion of previous researchers [12,38]. In the case of constant cement content, CPB strength decreases over time. According to Figure 6b, the 28th day σ_t is smaller than σ_t of the 3rd day and the 7th day when the solid mass concentration is constant. The ϵ showed no linear correlation with time regardless of the variation in cement content (*c*) and solid mass concentration (ω), and always reached its

maximum on the 7th day, shown in Figure 6c,d. Additionally, the ε showed the opposite trend for 7 days and 28 days curing ages with the increase in cement content. Moreover, ε on the 28th day decreased by 45% on average compared to the 7th day with the same solid mass concentration condition. This is because the tailings contained 11.90% S^{2-} , which is easily oxidized into sulfate ions and sulfate, leading to the formation of expansive products, gypsum and ettringite, and the decalcification of hydrated calcium silicate. This means that microcracks will be formed in the CPB and the hydration reaction will be inhibited, resulting in a great reduction in strength and peak strain with the extension of curing time.

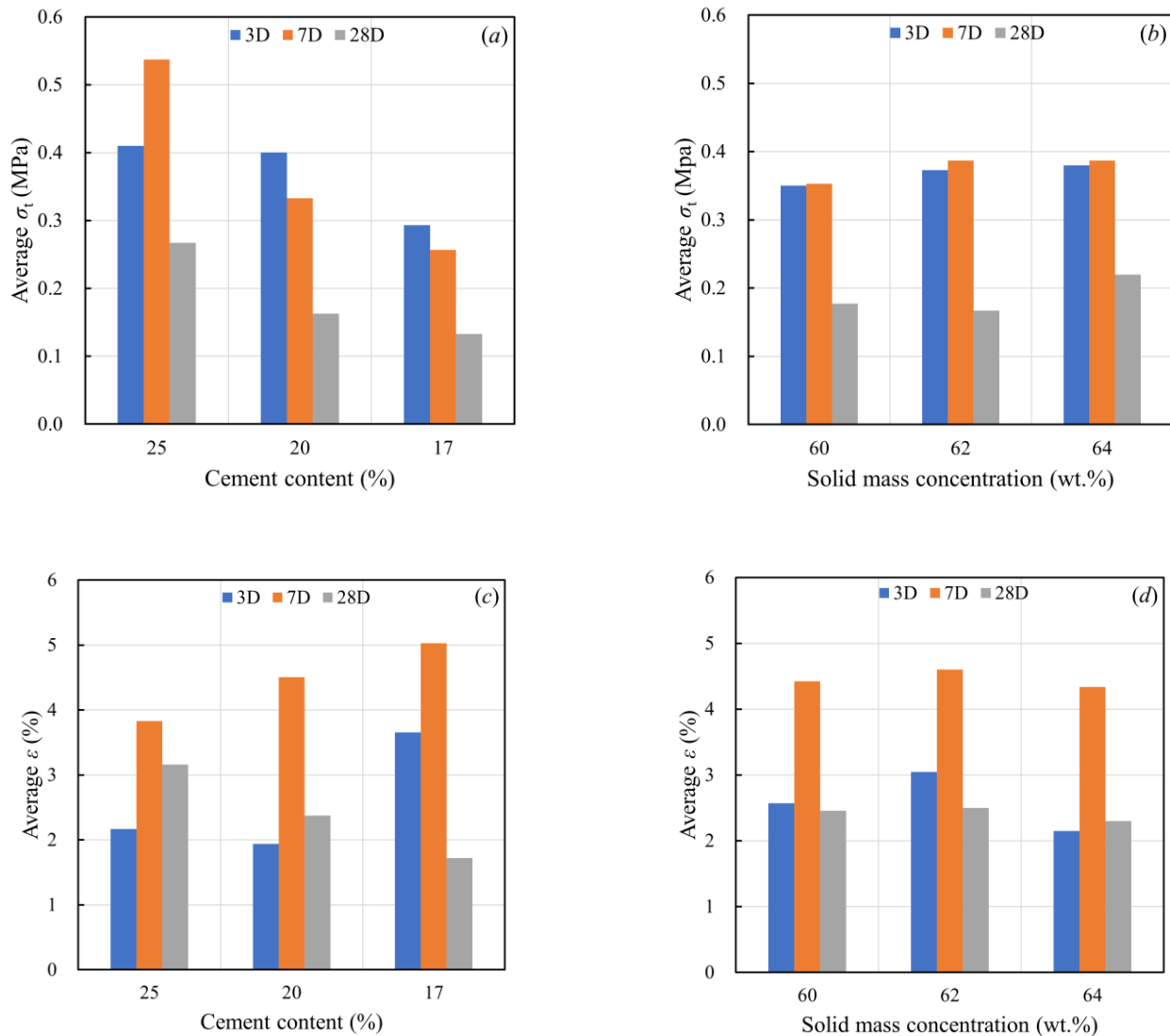


Figure 6. The influences of cement content and solid mass concentration on ITS and ε . (a) Average σ_t at different cement contents; (b) average σ_t at different solid mass concentration; (c) average ε at different cement contents; (d) average ε at different solid mass concentration.

3.3. Influence of RS Fibers on the Tensile Strength of CPB

According to Table 5, the peak tensile strengths of CCPB were 0.10~0.23 MPa, 0.12~0.22 MPa, and 0.16~0.26 MPa at 3, 7, and 28 days, respectively. The strength changed after adding RS fibers. When cured for 3 days, the peak tensile strengths of RSCPb were 0.28~0.50 MPa, 0.23~0.58 MPa for 7 days, and 0.11~0.32 MPa for 28 days. The relative errors (Re) of the tensile strength of RSCPb compared to CCPb were calculated according to Equation (2) [10].

$$Re_{\sigma} = \frac{\sigma_{t-A} - \sigma_{t-B}}{\sigma_{t-B}} \times 100\% \tag{2}$$

where σ_{t-A} and σ_{t-B} represent the peak tensile strength of specimens in groups A and B, respectively, and Re_{σ} represents the percentage of increase in the peak tensile strength of specimens in group A relative to group B.

It can be seen from Figure 7 that RS fibers can significantly increase the peak tensile strength of CPB in the first 7 days. A higher initial strength is beneficial to shorten the mining cycle of adjacent stopes and improve production efficiency [39,40]. Due to the differences in preparation formulas and curing ages between group A and B, Re_{σ} varied from -38.10% to 346.15% . Depending on the curing age, the increase in ITS of RSCPb ranged from 115.38% to 300.00% at 3 days curing age, 40.91% to 346.15% at 7 days, and -38.10% to 28.00% at 28 days. The enhancement in the ITS of CPB was evident, although the curing ages were only 3 and 7 days. For the 28-day curing age, the effect of adding RS fibers on the tensile strength of CPB is not significant.

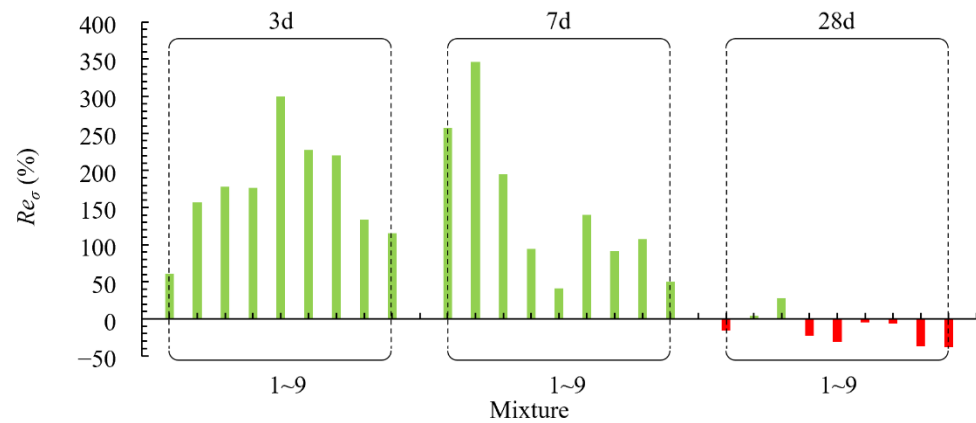


Figure 7. Re_{σ} of RSCPb for 3 days, 7 days, and 28 days curing ages.

The single factor analysis of the ITS of RSCPb was carried out for fiber content and length. Based on the results of the analysis, the effects of different RS fiber contents and lengths on the average ITS of the RSCPb are plotted in Figure 8. Figure 8a shows the average ITS of the RSCPb at different RS fiber addition masses. When the curing age was 3 days, the average ITS of the RSCPb decreased slightly with the increase in RS fiber content, and then increased by 30%. At the curing age of 7 days, the average ITS of the RSCPb first increased by 0.016 MPa and then decreased by 9.2% with the increase in RS fiber content. At 28 days of curing age, the average ITS of the RSCPb continued to increase slightly with the increase in fiber content. Figure 8b shows the effect of RS fiber length on the average ITS of the RSCPb. It can be seen that after being cured for 3 days, the average ITS decreased and then increased with the increase in the RS fiber length, and the tensile strength enhancement effect of the RSCPb with 3~5 cm RS fibers is the best. When the curing ages were 7 days and 28 days, the average ITS was affected by different fiber lengths in the same trend: the tensile strength of the RSCPb first increased and then decreased with increasing fiber length, and the specimens reached the maximum when the fiber length was 1~3 cm.

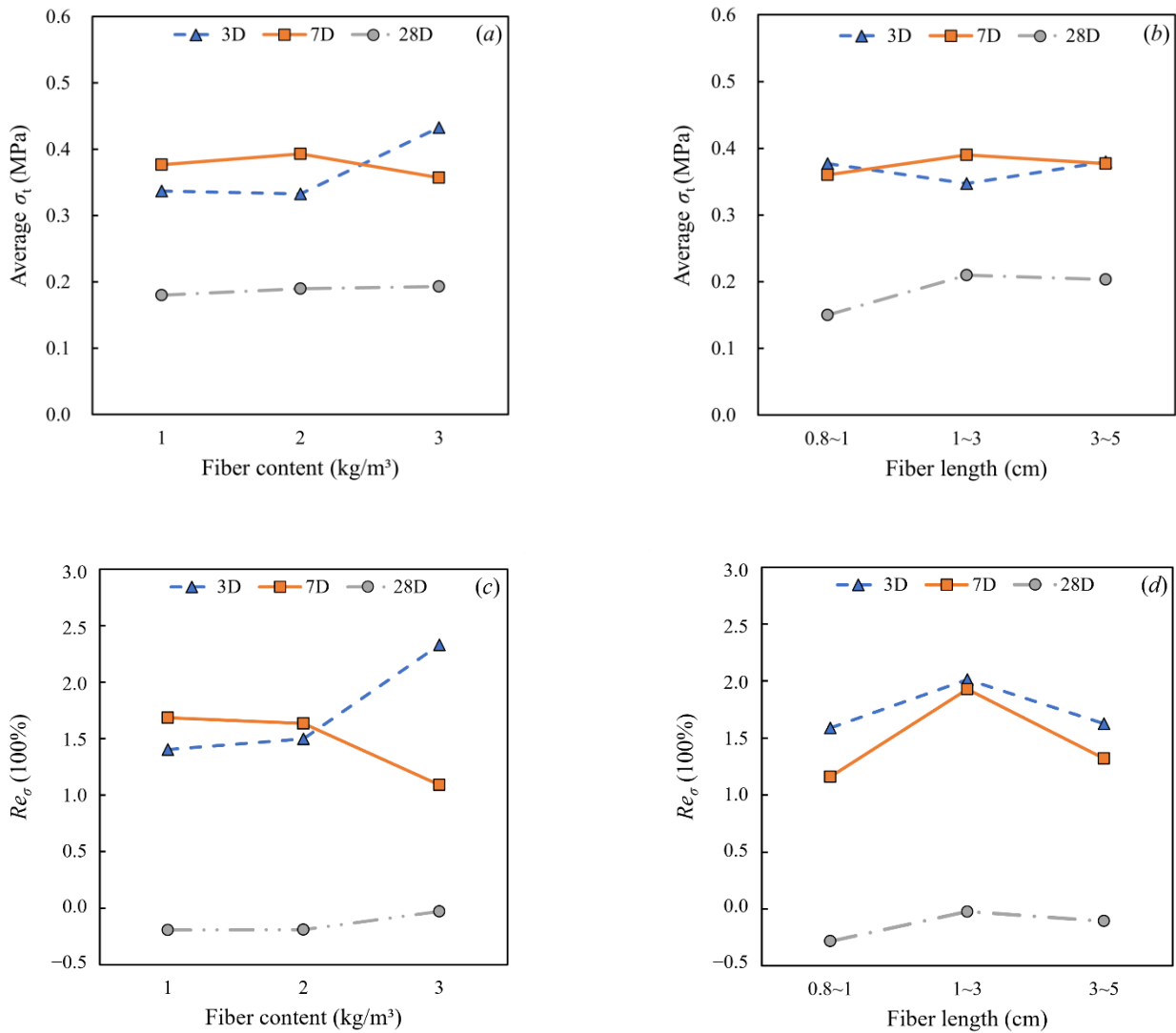


Figure 8. The influence of RS fiber on ITS and Re_{σ} . (a) Average σ_t at different RS fiber contents; (b) average σ_t at different RS fiber lengths; (c) average Re_{σ} at different RS fiber contents; (d) average Re_{σ} at different RS fiber lengths.

Figure 8c,d show the effects of RS fibers on Re_{σ} . When the curing ages were 3 and 28 days, as the content of RS fibers increased, Re_{σ} continued to increase; however, they gradually decreased at 7 days. Although the Re_{σ} with an RS fiber addition of 3 kg/m³ was lower than 2 kg/m³ cured for 3 days, the average tensile strength was still more than 100% higher than 0.173 MPa when no RS fiber was added. Re_{σ} increased first and then decreased with the increase in RS fiber length during the entire curing period. The effect of RS fibers on the long-term Re_{σ} of RSCPb is not obvious overall.

The strength enhancement of RS on the CPB is mainly reflected in the bridging effect of RS on the tailings aggregate and the toughness of RS itself. However, the addition of RS may also increase the degree of crack development within the CPB, which can weaken the strength enhancing effect of RS. In addition, the contribution of RS enhancement, aggregate cementation, and sulfation to the strength of the CPB does not occur simultaneously. Therefore, combining the effects of the above factors, the strength enhancement effect of the CPB shows fluctuating characteristics under the influences of different curing ages and RS additions. The relevant instructions have been added in the article.

3.4. Influence of RS Fibers on the Tensile Peak Strain of CPB

According to Table 5, the peak strain of group A ranged from 0.86% to 4.56% after curing for 3 days, and 3.74~5.87% and 1.38~3.67% after curing for 7 and 28 days, respectively. The peak strains of CCPB (group B) were 2.38~4.64%, 2.15~5.91%, and 2.67~5.82% when the curing ages were 3, 7, and 28 days, respectively. The relative errors of tensile peak strains of RSCPb compared with the CCPB are shown in Figure 9. In this section, the same method as that used for the calculation of Re_σ was used to calculate Re_ϵ . The Re_ϵ of the different specimens varied from -76.88% to 120.93% . According to the different curing ages, Re_ϵ varied from -76.88% to 16.03% on the 3rd day, from -36.72% to 120.93% on the 7th day, and from -70.67% to 12.73% on the 28th day. The results showed that the RS fibers did not significantly enhance the tensile peak strain of the CPB. Moreover, most of the data showed a decrease in peak strain.

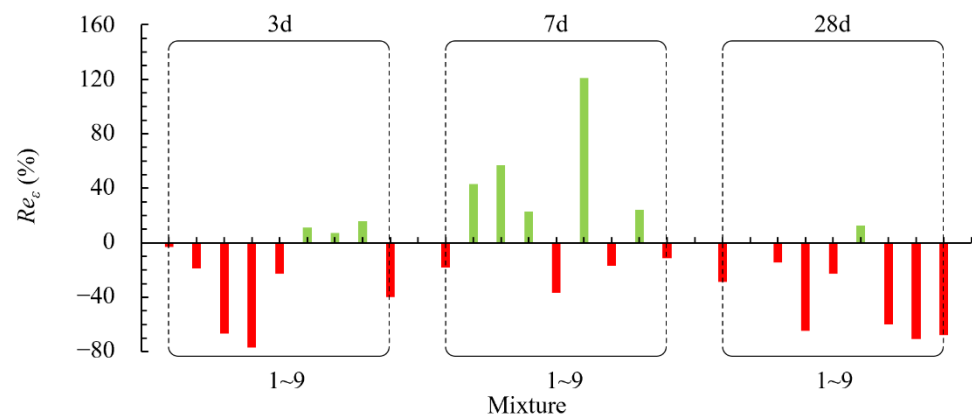


Figure 9. Re_ϵ of RSCPb for 3 days, 7 days, and 28 days curing ages.

To investigate the effects of RS fiber length and content, the average peak strains of the RSCPb at different contents and lengths are plotted in Figure 10. Figure 10a shows the effect of the added content of RS fibers on the peak strain of the RSCPb, which indicated that the peak strain had the same changing rule under the influence of different fiber lengths when the curing ages were 3 days and 28 days. With the increase in RS fiber content, the average ϵ of the RSCPb decreased and then increased. The peak strain reached the maximum value when the fiber content was 1 kg/m^3 , and the peak strains on the 3rd day and 28th day were 3.300% and 2.583%, respectively. At 7 days of curing age, the peak strain decreased continuously with the increase in fiber content. The maximum ϵ was 4.840% at a fiber content of 1 kg/m^3 .

Figure 10b shows the effect of RS fiber length on the peak tensile strain of the RSCPb. It can be seen that when the curing age is 3 days and 28 days, the peak strain trend is similar. As the fiber length increased, the peak strain of the RSCPb increased initially and decreased afterwards. The peak strain reached the maximum at fiber lengths of 1~3 cm, and the peak strain at 3 and 28 days of curing was 3.023% and 3.007%, respectively. At 7 days of curing age, the peak strain increased by 14.22% continuously with the increase in fiber length. The maximum peak strain was 4.764% when the fiber length was 3~5 cm. According to the analysis of the above data, the tensile peak strain trend of RSCPb with the addition of RS fibers is opposite to the trend with the fiber length.

The data in Figure 10c,d show that Re_ϵ shows a “V” shape as the RS fiber content changes from 1 to 3 kg/m^3 on the 3rd day and 28th day, however, ultimately it is less than 0%. On the 7th day, Re_ϵ keeps decreasing close to 0%. As the length of the RS fibers increases, Re_ϵ has an inverted “V” shape similar to the Re_σ with fiber length. With the addition of RS fibers, only a few RSCPb specimens increased in ϵ compared with CCPB. In terms of improving the strain of RSCPb, the RS fibers addition amount of 1 kg/m^3 and the length of 1~3 cm are the best values.

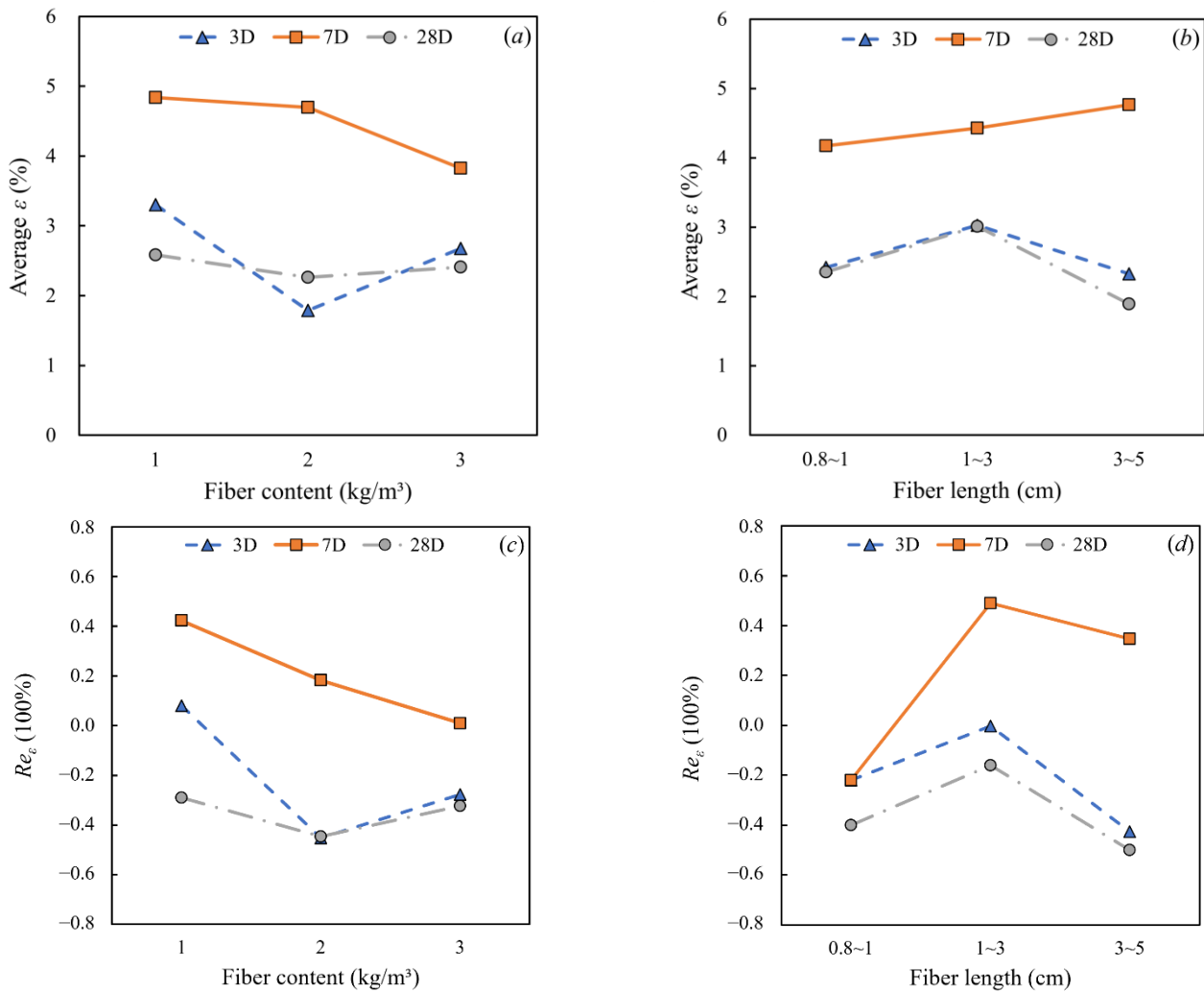


Figure 10. The influences of RS fiber on peak strain and Re_ϵ . (a) Average ϵ at different RS fiber contents; (b) average ϵ at different RS fiber lengths; (c) average Re_ϵ at different RS fiber contents; (d) average Re_ϵ at different RS fiber lengths.

3.5. SEM Results

The microstructure of RSCPb was observed. Figure 11 shows the SEM of specimens A2 and A8. The solid mass concentration of both is 62%; the difference is that the cement content of A2 is 25% and A8 is 17%. It can be seen from Figure 11 that the pore size of the A2 specimen is significantly smaller than that of A8 at the same observation scale, indicating that the hydration reaction products are more abundant at a higher cement content, which will wrap the RS fibers more tightly and contribute to enhancing the denseness and tensile properties of RSCPb. Moreover, a bent RS fiber that has a rough surface can be clearly seen in the SEM photograph of specimen A8 (Figure 11b). RS fibers uncoated by hydration products are present in RSCPb as weakly structured surfaces. The lower part of the fiber is fully wrapped by the hydration products, which indicates that the surface of the RS fibers can adsorb the hydration products and form a large-scale aggregate, which improves the compactness inside the CPb and, thus, the strength of the CPb.

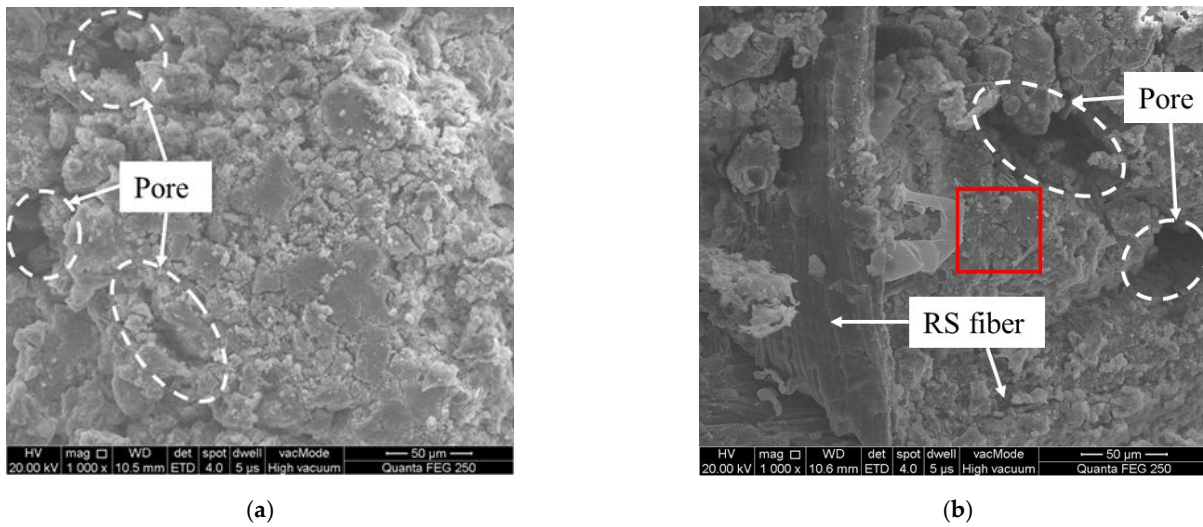


Figure 11. SEM images of A2 and A8 cured for 28 days. (a) A2; (b) A8.

The image in Figure 12 is an enlargement of the segment in the red box in Figure 11. It can be seen that C-S-H (spherical, flocculent), AFt (needle-like crystals), and C-H (hexagonal plates) [41] are interspersed and interlaced with each other. A large amount of ettringite, which is an expansive product generated by S^{2-} in the tailings [42], causes the formation of fractures inside the CPB, forming the microcrack structure shown in Figure 12. The cracks connect and develop when subjected to tensile forces, which is one of the main reasons for its brittle damage and reduced tensile strain.

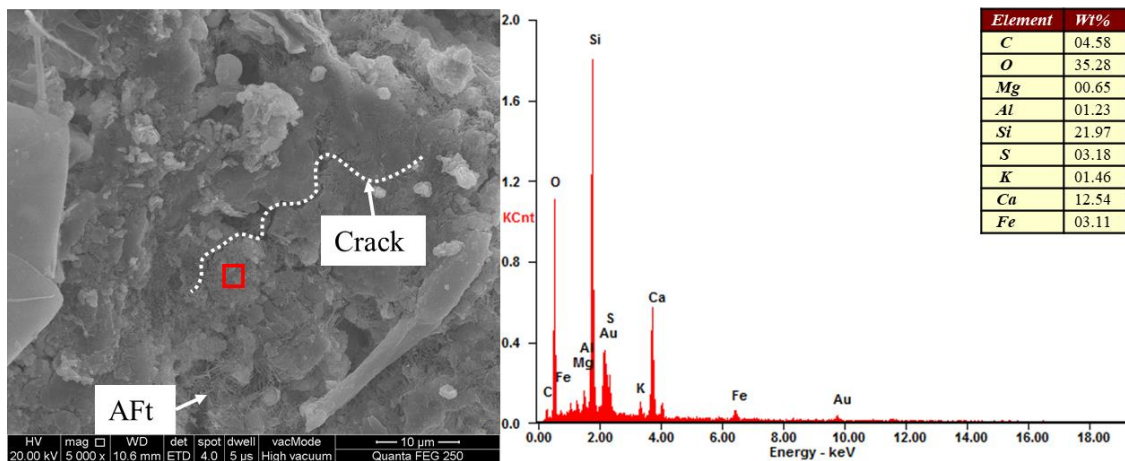


Figure 12. SEM images of A2 and A8 cured for 28 days.

In previous studies, RS fibers have been shown to improve the compressive and tensile properties of the backfill, and the low price and wide availability of RS make it feasible to use RS fibers as a backfill additive material. The use of RS fibers to backfill can reduce the amount of cement and thus the cost, while maintaining the strength in the early curing time. The composition of RS is dominated by organic matter, and the organic component can be further removed by pyrolysis or alkali treatment, thus increasing the inertness of the RS fiber may further improve the strength of the backfill [26,31]. However, the removal of the fiber structure will reduce the toughness of the RS, which is a double-edged sword. In addition, further resizing of the RS fibers by reducing the length and narrowing the diameter may further improve the linkage effect between the RS fibers and the aggregate, thus improving the strength of the backfill and reducing its effect on the flowability of the backfill slurry, which will be further worked on in subsequent studies.

4. Conclusions

The tensile response of the RSCPb was analyzed, and the tensile strength and strain of RSCPb were studied and discussed based on the Brazilian split tensile test. The main conclusions that were obtained are as follows:

- (1) Tensile stress–strain curves indicate that RSCPb has a larger elastic modulus. ITS of RSCPb is greater than CCPb. Most of the RSCPb and CCPb specimens are characterized by brittle fracture, of which only a small proportion of the RSCPb specimens exhibit residual strength characteristics. High sulfur (S^{2-}) content in the tailings has a negative impact on the long-term strength of RSCPb.
- (2) The ITS of the RSCPb increased by -38.10% to 346.15% compared to CCPb; ITS was generally improved in the initial 7 days and generally lowered at 28 days of curing. Meanwhile, the tensile strain increased by -33.54% to 277.97% , which was generally lower compared to CCPb, indicating that RSCPb is still a brittle material. The analysis results showed that CPb specimens' brittleness was enhanced with the addition of fibers.
- (3) The effects of RS fiber content and length on RSCPb tensile strength and strain are not linear, and different curing ages lead to different effects. In engineering applications, the appropriate formulation should be selected based on the requirements.
- (4) The rough surface of RS fibers can adsorb the hydration products to form large aggregates; moreover, increasing the cement content helps to enhance the CPb denseness. Furthermore, the calcium alumina in the hydration products has a negative effect on the mechanical properties of RSCPb.

Author Contributions: Conceptualization, X.C. and Z.L.; methodology, X.C.; software, Z.L.; validation, X.S. and X.C.; formal analysis, X.C. and Z.L.; investigation, X.C.; resources, X.S.; data curation, X.C.; writing—original draft preparation, Z.L.; writing—review and editing, X.C.; visualization, Z.L.; supervision, X.S.; project administration, X.S. and X.C.; funding acquisition, X.C. and X.S. All authors have read and agreed to the published version of the manuscript.

Funding: This research was funded by the National Natural Science Foundation Project of China, grant number 51874350 and Hunan Provincial Natural Science Foundation Project, grant number 2021JJ40733.

Institutional Review Board Statement: Not applicable.

Informed Consent Statement: Not applicable.

Data Availability Statement: The data are contained within the article.

Acknowledgments: We are grateful to Shenzhen Zhongjin Lingnan Non-ferrous Metal Company Limited for providing us with the tailings and Central South University for providing us with the experimental platform.

Conflicts of Interest: The authors declare no conflict of interest.

References

1. Chen, Q.-S.; Zhang, Q.-L.; Fourie, A.; Chen, X.; Qi, C.-C. Experimental investigation on the strength characteristics of cement paste backfill in a similar stope model and its mechanism. *Constr. Build. Mater.* **2017**, *154*, 34–43. [[CrossRef](#)]
2. Chen, X.; Shi, X.; Zhou, J.; Chen, Q.; Yang, C. Feasibility of Recycling Ultrafine Leaching Residue by Backfill: Experimental and CFD Approaches. *Minerals* **2017**, *7*, 54. [[CrossRef](#)]
3. Deng, D.Q.; Liu, L.; Yao, Z.L.; Song, K.I.L.; Lao, D.Z. A practice of ultra-fine tailings disposal as filling material in a gold mine. *J. Environ. Manag.* **2017**, *196*, 100–109. [[CrossRef](#)] [[PubMed](#)]
4. Chen, X.; Shi, X.; Zhou, J.; Du, X.; Chen, Q.; Qiu, X. Effect of overflow tailings properties on cemented paste backfill. *J. Environ. Manag.* **2019**, *235*, 133–144. [[CrossRef](#)] [[PubMed](#)]
5. Li, H.; Gao, P.; Xu, F.; Sun, T.; Zhou, Y.; Zhu, J.; Peng, C.; Lin, J. Effect of Fine Aggregate Particle Characteristics on Mechanical Properties of Fly Ash-Based Geopolymer Mortar. *Minerals* **2021**, *11*, 897. [[CrossRef](#)]
6. Chalangan, N.; Farzampour, A.; Paslar, N.; Fatemi, H. Experimental investigation of sound transmission loss in concrete containing recycled rubber crumbs. *Adv. Concr. Constr.* **2021**, *11*, 447–454. [[CrossRef](#)]

7. Chalangan, N.; Farzampour, A.; Paslar, N. Nano silica and metakaolin effects on the behavior of concrete containing rubber crumbs. *CivilEng* **2020**, *1*, 264–274. [[CrossRef](#)]
8. Li, E.; Zhou, J.; Shi, X.; Jahed Armaghani, D.; Yu, Z.; Chen, X.; Huang, P. Developing a hybrid model of salp swarm algorithm-based support vector machine to predict the strength of fiber-reinforced cemented paste backfill. *Eng. Comput.* **2020**, *37*, 3519–3540. [[CrossRef](#)]
9. Zhu, C.; Zhou, N.; Guo, Y.; Li, M.; Cheng, Q. Effect of Doped Glass Fibers on Tensile and Shear Strengths and Microstructure of the Modified Shotcrete Material: An Experimental Study and a Simplified 2D Model. *Minerals* **2021**, *11*, 1053. [[CrossRef](#)]
10. Chen, X.; Shi, X.; Zhou, J.; Chen, Q.; Li, E.; Du, X. Compressive behavior and microstructural properties of tailings polypropylene fibre-reinforced cemented paste backfill. *Constr. Build. Mater.* **2018**, *190*, 211–221. [[CrossRef](#)]
11. Chen, X.; Shi, X.; Zhou, J.; Yu, Z. Influence of Polypropylene Fiber Reinforcement on Tensile Behavior and Failure Mode of Tailings Cemented Paste Backfill. *IEEE Access* **2019**, *7*, 69015–69026. [[CrossRef](#)]
12. Cristelo, N.; Cunha, V.M.C.F.; Topa Gomes, A.; Araújo, N.; Miranda, T.; Lurdes Lopes, M.d. Influence of fibre reinforcement on the post-cracking behaviour of a cement-stabilised sandy-clay subjected to indirect tensile stress. *Constr. Build. Mater.* **2017**, *138*, 163–173. [[CrossRef](#)]
13. Juradin, S.; Boko, I.; Netinger Grubeša, I.; Jozić, D.; Mrakovčić, S. Influence of different treatment and amount of Spanish broom and hemp fibres on the mechanical properties of reinforced cement mortars. *Constr. Build. Mater.* **2021**, *273*, 121702. [[CrossRef](#)]
14. Jiang, C.; Fan, K.; Wu, F.; Chen, D. Experimental study on the mechanical properties and microstructure of chopped basalt fibre reinforced concrete. *Mater. Des.* **2014**, *58*, 187–193. [[CrossRef](#)]
15. Long, W.; Wang, Y. Effect of pine needle fibre reinforcement on the mechanical properties of concrete. *Constr. Build. Mater.* **2021**, *278*, 122333. [[CrossRef](#)]
16. Mansouri, I.; Shahheidari, F.S.; Hashemi, S.M.A.; Farzampour, A. Investigation of steel fiber effects on concrete abrasion resistance. *Adv. Concr. Constr.* **2020**, *9*, 367–374.
17. Yoo, D.-Y.; Banthia, N. Impact resistance of fiber-reinforced concrete—A review. *Cem. Concr. Compos.* **2019**, *104*, 103389. [[CrossRef](#)]
18. Zhi, Y.; Shi, X.-Z.; Xin, C.; Jian, Z.; Qi, C.-C.; Chen, Q.-S.; Rao, D.-J. Artificial intelligence model for studying unconfined compressive performance of fiber-reinforced cemented paste backfill. *Trans. Nonferrous Met. Soc. China* **2021**, *31*, 1087–1102.
19. Shang, X.; Yang, J.; Song, Q.; Wang, L. Efficacy of modified rice straw fibre on properties of cementitious composites. *J. Clean. Prod.* **2020**, *276*, 124184. [[CrossRef](#)]
20. Logeswaran, J.; Shamsuddin, A.H.; Silitonga, A.S.; Mahlia, T.M.I. Prospect of using rice straw for power generation: A review. *Environ. Sci. Pollut. Res.* **2020**, *27*, 25956–25969. [[CrossRef](#)]
21. Ma, Y.; Shen, Y.; Liu, Y. State of the art of straw treatment technology: Challenges and solutions forward. *Bioresour. Technol.* **2020**, *313*, 123656. [[CrossRef](#)]
22. Van Hung, N.; Maguyon-Detras, M.C.; Migo, M.V.; Quilloy, R.; Balingbing, C.; Chivenge, P.; Gummert, M. Rice Straw Overview: Availability, Properties, and Management Practices. In *Sustainable Rice Straw Management*; Springer: Cham, Switzerland, 2020; pp. 1–13.
23. Chabi, E.; Doko, V.; Hounkpè, S.P.; Adjovi, E.C. Study of cement composites on addition of rice husk. *Case Stud. Constr. Mater.* **2020**, *12*, e00345. [[CrossRef](#)]
24. Marques, B.; Tadeu, A.; Almeida, J.; Antonio, J.; de Brito, J. Characterisation of sustainable building walls made from rice straw bales. *J. Build. Eng.* **2020**, *28*, 101041. [[CrossRef](#)]
25. Sathiparan, N.; De Zoysa, H. The effects of using agricultural waste as partial substitute for sand in cement blocks. *J. Build. Eng.* **2018**, *19*, 216–227. [[CrossRef](#)]
26. Chen, X.; Shi, X.; Zhou, J.; Yu, Z.; Huang, P. Determination of mechanical, flowability, and microstructural properties of cemented tailings backfill containing rice straw. *Constr. Build. Mater.* **2020**, *246*, 118520. [[CrossRef](#)]
27. Ashour, T.; Morsy, M.; Korjenic, A.; Fischer, H.; Khalil, M.; Sesto, E.; Orabi, M.; Yehia, I. Engineering Parameters of Rice Straw Concrete with Granulated Blast Furnace Slag. *Energies* **2021**, *14*, 343. [[CrossRef](#)]
28. Wang, S.; Song, X.; Chen, Q.; Wang, X.; Wei, M.; Ke, Y.; Luo, Z. Mechanical properties of cemented tailings backfill containing alkalinized rice straw of various lengths. *J. Environ. Manag.* **2020**, *276*, 111124. [[CrossRef](#)]
29. Chen, Q.; Zhang, Q.; Xiao, C.; Chen, X. Backfilling behavior of a mixed aggregate based on construction waste and ultrafine tailings. *PLoS ONE* **2017**, *12*, e0179872. [[CrossRef](#)]
30. Wu, J.; Feng, M.; Chen, Z.; Mao, X.; Han, G.; Wang, Y. Particle Size Distribution Effects on the Strength Characteristic of Cemented Paste Backfill. *Minerals* **2018**, *8*, 322. [[CrossRef](#)]
31. Chen, X.; Shi, X.; Zhou, J.; Li, E.; Qiu, P.; Gou, Y. High strain rate compressive strength behavior of cemented paste backfill using split Hopkinson pressure bar. *Int. J. Min. Sci. Technol.* **2021**, *31*, 387–399. [[CrossRef](#)]
32. Wei, L.; Chai, S.X.; Zhang, H.Y.; Shi, Q. Mechanical properties of soil reinforced with both lime and four kinds of fiber. *Constr. Build. Mater.* **2018**, *172*, 300–308. [[CrossRef](#)]
33. Xie, X.; Gou, G.; Wei, X.; Zhou, Z.; Jiang, M.; Xu, X.; Wang, Z.; Hui, D. Influence of pretreatment of rice straw on hydration of straw fiber filled cement based composites. *Constr. Build. Mater.* **2016**, *113*, 449–455. [[CrossRef](#)]
34. Farzampour, A. Temperature and humidity effects on behavior of grouts. *Adv. Concr. Constr.* **2017**, *5*, 659. [[CrossRef](#)]
35. Farzampour, A. Compressive behavior of concrete under environmental effects. In *Compressive Strength of Concrete*; IntechOpen: London, UK, 2019; pp. 91–104.

36. Huang, Z.; Zhang, Y.; Li, Y.; Zhang, D.; Yang, T.; Sui, Z.; Vieira, C.S. Determining Tensile Strength of Rock by the Direct Tensile, Brazilian Splitting, and Three-Point Bending Methods: A Comparative Study. *Adv. Civ. Eng.* **2021**, *2021*, 5519230. [[CrossRef](#)]
37. American Society for Testing and Materials. *Standard Test Method for Splitting Tensile Strength of Intact Rock Core Specimens*; ASTM International: West Conshohocken, PA, USA, 2016.
38. Jafari, M.; Grabinsky, M. Effect of hydration on failure surface evolution of low sulfide content cemented paste backfill. *Int. J. Rock Mech. Min. Sci.* **2021**, *144*, 104749. [[CrossRef](#)]
39. Ercikdi, B.; Baki, H.; Izki, M. Effect of desliming of sulphide-rich mill tailings on the long-term strength of cemented paste backfill. *J. Environ. Manag.* **2013**, *115*, 5–13. [[CrossRef](#)] [[PubMed](#)]
40. Nasir, O.; Fall, M. Coupling binder hydration, temperature and compressive strength development of underground cemented paste backfill at early ages. *Tunn. Undergr. Space Technol.* **2010**, *25*, 9–20. [[CrossRef](#)]
41. Lv, X.; Shi, Y.; Dong, Y.; Gao, Z.; Li, B. The Performance and Mechanism Analysis of Cement Pastes Added to Aluminum Sulfate-Based Low-Alkali Setting Accelerator. *Adv. Mater. Sci. Eng.* **2017**, *2017*, 8906708. [[CrossRef](#)]
42. Chen, X.; Shi, X.; Zhang, S.; Chen, H.; Zhou, J.; Yu, Z.; Huang, P. Fiber-Reinforced Cemented Paste Backfill: The Effect of Fiber on Strength Properties and Estimation of Strength Using Nonlinear Models. *Materials* **2020**, *13*, 718. [[CrossRef](#)]